Characterization of elastomeric scaffolds developed for tissue engineering applications by compression and nanoindentation tests, μ-Raman and μ-Brillouin spectroscopies

Geraldine Rohman, Salah Ramtani, Sylvie Changotade, Credson Langueh, Didier Lutomski, Yves Roussigné, Florent Tetard, Frederic Caupin, Philippe Djemia

Research Article | Vol. 10, No. 4 | 1 Apr 2019 | BIOMEDICAL OPTICS EXPRESS 1649
Biomedical Optics EXPRESS

Characterization of elastomeric scaffolds developed for tissue engineering applications by compression and nanoindentation tests, μ-Raman and μ-Brillouin spectroscopies

GÉRALDINE ROHMAN,[1,2,*] SALAH RAMTANI,[1,2] SYLVIE CHANGOTADE,[1,2] CREDSON LANGUEH,[1,2] DIDIER LUTOMSKI,[1,2] YVES ROUSSIGNÉ,[3] FLORENT TÉTARD,[3] FRÉDERIC CAUPIN,[4] AND PHILIPPE DJEMIA[2,3]

[1] *Laboratoire Chimie, Structures, Propriétés de Biomatériaux et d'Agents Thérapeutiques CSPBAT UMR7244 CNRS, Université Paris 13, Villetaneuse , France*
[2] *Institut Interdisciplinaire des Sciences Expérimentales, Université Paris 13, Villetaneuse, France*
[3] *Laboratoire des Sciences des Procédés et des Matériaux LSPM-CNRS 3407, Sorbonne Paris Cité, Villetaneuse, France*
[4] *Université de Lyon, Université Claude Bernard, Lyon 1, CNRS, Institut Lumiére Matiére, F-69622, Villeurbanne, France*
[*] *geraldine.rohman@univ-paris13.fr*

Abstract: In tissue engineering, porous biodegradable scaffolds are developed with morphological, chemical and mechanical properties to promote cell response. Therefore, the scaffold characterization at a (sub)micrometer and (bio)molecular level is paramount since cells are sensitive to the chemical signals, the rigidity, and the spatial structuring of their microenvironment. In addition to the analysis at room temperature by conventional quasi-static (0.1–45 Hz) mechanical tests, the ultrasonic (10 MHz) and μ-Brillouin inelastic light scattering (13 GHz) were used in this study to assess the dynamical viscoelastic parameters at different frequencies of elastomeric scaffolds. Time-temperature superposition principle was used to increase the high frequency interval (100 MHz–100 THz) of Brillouin experiments providing a mean to analyse the viscoelastic behavior with the fractional derivative viscoelastic model. Moreover, the μ-Raman analysis carried out simultaneously during the μ-Brillouin experiment, gave the local chemical composition.

1. Introduction

The aim of tissue engineering is to develop porous biodegradable structures (scaffolds) adequate for the migration, the adhesion, the proliferation and the differentiation of cells seeded in the material before the implantation or recruited from the implantation site [1]. It is well known that the scaffold properties, such as surface chemistry, porosity and mechanical properties, affect cells response [2-5]. Indeed, surface chemistry has a huge impact on the local adhesion, the cell spreading and overall biocompatibility [6], while the mechanical properties in relation to the porosity influence the cell form, proliferation, and cortical stiffness [7]. As a consequence, it is of very high importance to be able to deeply characterize scaffolds at (sub)micrometer and (bio)molecular levels. For this purpose, μ-Raman spectroscopy is a technology increasingly used in the field of biomedical research. This technique uses the inelastic scattering of light by matter to give informations related to the (bio)chemical composition of cells, tissues, and scaffolds [8]. Regarding μ-Brillouin spectroscopy, this non-destructive and non-invasive technique has only been considered recently for the biomedical field [9]. Based on the analysis of the frequency spectrum (position and full width at half maximum of the inelastic peaks) of the light scattering

#353355 https://doi.org/10.1364/BOE.10.001649
Journal © 2019 Received 3 Dec 2018; revised 10 Feb 2019; accepted 17 Feb 2019; published 5 Mar 2019
Corrected: 7 Mar 2019

Biomedical Optics EXPRESS

induced by the coupling of a bulk acoustic wave with the light propagating in the matter [10], it is possible to quantify locally the viscoelastic properties of cells and biomaterials.

Polyurethane-based scaffolds have been increasingly used in tissue engineering since the elastomeric character offers an alternative to conventional rigid thermoplastic scaffolds [11]. Indeed, elastomeric scaffolds can be used to regenerate soft and dynamic tissues such as skin, tendons, and muscles, since the mismatch of Young moduli is reduced and the material is able to recover large mechanical deformations. CSPBAT has developed biodegradable poly(ester-urethane)-based scaffolds (PCLU) that can support the adhesion of cells [12]. This study shows the potential of the combination use of the nanoindentation tests, the pulse-echo ultrasonic technique and of the μ-Brillouin spectroscopy *vs* temperature to assess some dynamical viscoelastic parameters of elastomeric scaffolds at very different frequencies (Hz–100 THz). Moreover, the scaffold longitudinal moduli obtained by Brillouin spectroscopy are compared with the experimental data of conventional quasi-static (0.1 Hz) mechanical tests in an uni-axial stress mode of compression, as well as in a tri-axial stress mode of compression to mimic the containment to which the material can be subjected after implantation in cavitary defects. Finally, the scaffold chemical properties were also followed by an original coupled μ-Raman–μ-Brillouin spectroscopies system and compared with the results obtained from infrared spectroscopy.

2. Methods

2.1. Materials

All solvents were purchased from Fisher and used as received. Triol poly(ϵ-caprolactone) oligomers, hexamethylene diisocyanate, Span 80, dibutyltin dilaurate, were purchased from Sigma-Aldrich.

2.2. Elaboration and characterization of PCLU scaffolds

PCLU scaffolds were obtained through a high internal phase emulsion process named polyHIPE, and characterized by determination of their density, porosity and pore inter-connectivity, as previously described [12]. The glass transition temperature was estimated below - 80 °C by differential scanning calorimetry.

The scaffold morphology was monitored using an environmental scanning electron microscope (ESEM TM3000 - Hitachi).

The chemical composition of PCLU scaffolds was monitored by Fourier-transformed infrared spectroscopy (FTIR Nicolet 380 - Thermo Scientific) in an attenuated total reflectance mode (ATR - Smart Omni Sampler) within the range 500-4000 cm^{-1} with a resolution of 4 cm^{-1}, as well as by μ-Raman analysis. Here, we used an original setup that enabled to perform simultaneously, μ-Raman and μ-Brillouin local analysis. Raman spectra were recorded with the same microscope setup from the backscattered light with a Raman spectrometer (Horiba Jobin-Yvon iHR 550, 300 lines mm^{-1} grating, 50 μm entrance slit). More details on this setup can be found in Ref. [13].

The number average molecular weight between cross-links $\bar{M}_c$ of a porous cross-linked structure can be determined through swelling measurement. For this purpose, PCLU scaffolds were immersed in toluene at room temperature up to swelling equilibrium. At the end of the immersion period, PCLU scaffolds were removed from toluene, rapidly wiped to remove solvent excess at the sample surface, and weighted to obtain the wet mass of the scaffold. The apparent polymer volume fraction in the porous system υ_{2app} was calculated using Eq. (1) [14]:

$$\upsilon_{2app} = \frac{m_{dry} \times \rho_s}{m_{dry} \times \rho_{non-porous} \times \left(\frac{\rho_s}{\rho_{porous}} - 1\right) + m_{wet} \times \rho_{non-porous}} \quad (1)$$

where m_{dry} is the mass of the scaffold before swelling, m_{wet} is the mass of the scaffold after swelling, ρ_s is the density of the swelling agent (toluene), $\rho_{non-porous}$ is the density of the

Biomedical Optics EXPRESS

non-porous PCLU network prepared in the same conditions compared to the porous scaffold without the addition of water, and ρ_{porous} is the density of the porous PCLU scaffold.

Thereafter, the actual polymer volume fraction υ_{2s}, which is related to the measured apparent polymer volume fraction υ_{2app} determined from Eq. (1) and the porosity P of the scaffold, can be expressed by Eq. (2) [14]:

$$\frac{1}{\upsilon_{2s}} = \frac{1}{\upsilon_{2app}} - \frac{P}{1-P} \tag{2}$$

Finally, the number average molecular weight between cross-links $\bar{M_c}$ is calculated using the Flory- Rehner equation, Eq. (3) [15]:

$$\bar{M_c} = -\frac{V_s \times \left(\upsilon_{2s}^{1/3} - \frac{\upsilon_{2s}}{2}\right)}{\bar{\upsilon} \times \left[ln(1-\upsilon_{2s}) + \upsilon_{2s} + \chi \times \upsilon_{2s}^2\right]} \tag{3}$$

where V_s is the molar volume of the swelling agent (toluene), $\bar{\upsilon}$ is the specific volume of the polymer, χ is the Flory polymer-solvent interaction parameter calculated from the solubility parameters using Bristow and Watson equation, Eq. (4) [15]:

$$\chi = 0.34 + \frac{V_s}{RT} \times \left(\delta_s - \delta_p\right)^2 \tag{4}$$

where V_s is the molar volume of the solvent (toluene), R is the universal gas constant, T is the absolute temperature, δ_s is the solubility parameter of the solvent, and δ_p is the solubility parameter of the polymer network calculated using the group contribution method based on Van Krevelen′s molar attraction constants [16].

2.3. Compression tests

The mechanical behavior of PCLU scaffolds was determined by compression test carried out in the axial direction to the foam rise with a universal machine. Specimens′ dimensions were 8 *mm* in height and 18 *mm* in diameter. Compressive properties were determined in a 500 *N* force range, a 7 *mm* displacement range, and a displacement rate of 5 $mm.min^{-1}$. The stress/strain relation was computer-recorded and processed using Realview 3.0 software. The linear regression procedure was applied for determination of elastic moduli at the beginning of the curve for the porous PCLU scaffold, and at the end of the curve for the non-porous PCLU material. The typical acquisition time of the linear slope (strain increasing of 0.05–0.1) was of ~10 s corresponding to a 1/10 Hz frequency for this test. The mechanical behavior of confined PCLU scaffolds was also determined in a similar experiment except that the scaffold was confined in a hole of 16 *mm* in diameter.

2.4. Nanoindentation tests

The mechanical properties of the films were determined from load-displacement curves obtained with a MTS Nanoindenter XP apparatus. Nanoindentation tests with continuous stiffness measurement (CSM) were carried out for indentation modulus E_{IT} measurements. All experiments were performed with a diamond-type Berkovich indenter. The strain rate and the frequency oscillation of the displacement was varied in the range 0.01–0.2 s^{-1} and 1–45 Hz, respectively. The parameters set for the measurement are a depth of 2 μm and an amplitude of 2 nm. Each value was computed as the average of 20 measurements in the range of 0–2000 nm penetration depth by using the Oliver and Pharr method [17].

Biomedical Optics EXPRESS

2.5. Ultrasound echoes

The pulse-echo technique was employed to measure the longitudinal sound velocity V_L from the time of flight of the echoes that are traveling forth and back along the length of two PCLU dense samples (3.5 mm and 3.8 mm) of the cylindrical shaped sample with 10 mm in diameter and opposite parallel faces. The travel time of ultrasonic waves propagating through the sample with a 10 MHz frequency was measured using a Sofranel D20 ultrasound device with a measuring time accuracy of 0.5 ns. The accuracy for the sound velocity is about 0.1 %. Acoustic attenuation was not measured.

2.6. μ-Brillouin spectroscopy and time-temperature superposition principle

The longitudinal sound velocity V_L was measured locally (laser spot size of a few μm^2) by the μ-Brillouin light scattering technique [8, 9, 13] in the backscattering geometry with a long-working-distance (6 mm) x100 objective (Mitutoyo plan-apo infinity corrected (N.A. 0.7) and an entrance pinhole = 300 μm for the Brillouin spectrometer. More details about the setup and procedure are given in Ref. [13]. We just give here a brief summary. For Brillouin scattering experiments, the incoming light from a single longitudinal mode laser at λ_L = 532 nm (Coherent Verdi 6) was coupled to the microscope. The intensity was kept below 100 mW at the sample. The light back-scattered into the objective was analyzed with a 2x3-pass tandem Fabry-Perot interferometer (Sandercock TFP-1) to record its Brillouin spectrum. The wavevector modulus k of the probe bulk acoustic wave is defined by:

$$k = 4\pi n/\lambda_L \tag{5}$$

n ~1.6 ± 0.05 is the refractive index of the PCLU material. From the measurement of the Brillouin frequency shift f_B of the inelastic scattered light, the sound velocity V_L is calculated by:

$$V_L = f_B \lambda_L / 2n \tag{6}$$

The intensity as a function of the frequency shift f was fitted with a damped harmonic oscillator (DHO) function considering a Brillouin frequency shift f_B and a full-width at half-maximum Γ_B, convoluted with the instrumental response well reproduced by a Gaussian profile (line-width 418 MHz). The dynamical longitudinal viscosity η can be estimated from the natural line-width (Γ_B) obtained after deconvolution of the instrumental line-width, by the following relation:

$$\eta = \rho \Gamma_B / k^2 \tag{7}$$

The complex longitudinal modulus $M = M' + iM$", M' being the storage modulus and M" the loss modulus, is defined by:

$$M = \rho V_L^2 + i\eta 2\pi f_B \tag{8}$$

The same mechanical characterization (i.e. the longitudinal modulus M) carried out at room temperature (20 °C) by varying the frequency could only be applied for 10 MHz (ultrasound echoes) and 13 GHz (BLS). Nevertheless, an attempt to estimate the high frequency behavior of M is accessible via the time-temperature superposition principle (TTSP) by performing BLS as a function of the temperature. It states that the effect of changing the temperature is the same as applying a multiplication factor to the timescale (frequency), $a_T(T, T_r)$, which is given by the William-Landel-Ferry (WLF) equation [18]:

$$ln(a_T(T, T_r)) = -\frac{C_1(T - T_r)}{C_2 + (T - T_r)} \tag{9}$$

T_r is the reference temperature (here, 20 °C) at which we calculate the translated frequency $a_T(T, T_r) * f$ with the modulus $M(f, T)$, in case of a thermo-rheologically simple polymer

Biomedical Optics EXPRESS

(i.e. $M(f,T) = M(a_T(T,T_r) * f, T_r)$) [19]. In some cases, for heterogeneous materials with multiple relaxation times, it can be necessary to consider a vertical shift $b_T(T,T_r)$ for the modulus. This shift is related to thermal expansion effects, which for most polymers can be neglected. Nevertheless, it can be theoretically evaluated if the thermal expansion of the polymer is known [19], but it is not our case. A direct calculation considering the minimisation of a criterion based on the Kramers-Kronig relations has also been proposed by Rouleau et al. [20]. To partially overcome this difficulty, we considered the closest modulus measured at 10 MHz and room temperature by ultrasounds, as a reference, through which the used viscoelastic model have to go through and as closest as possible to the higher frequency data obtained by BLS. Similar methods in which the shifts coefficients are identified along the parameters of a viscoelastic model have already been proposed [21, 22] This concept works well for amorphous and self-adhesive rubber, as an example, and allows for the construction of master curves of the complex modulus on a broad frequency scale [18, 23].

3. Results and discussions

3.1. Scaffold elaboration and structural characterization

Various elastomeric polymers have been proposed as scaffolds for tissue engineering. Among available biocompatible and biodegradable elastomers, polyurethane, poly(ester-urethane) and poly(ester-urethane-urea) are of much interest since they can be synthesized with various chemical and mechanical properties, as well as with various degradation rates [11]. In this study, poly(ester-urethane)-based scaffolds (PCLU) were elaborated from a high internal phase emulsion in which oligoesters contained in the continuous phase were cross-linked. Depending of the emulsion parameters, various multi-scale and interconnected porosities can be obtained [12]. More specifically here, PCLU scaffolds were designed to present a 85.1% open-porosity that did not contain closed voids, and pore sizes ranging from below 150 to 1800 μm (Fig. 1(a) - left and Fig. 1(b)). A non-porous material, which is transparent, was also prepared in the same conditions compared to the PCLU scaffold without the addition of water (Fig. 1(a) - right).

It was demonstrated that during the scaffold elaboration, side reactions with water arose leading to the formation of urea moieties [12]. Thereby, the determination of the scaffold chemical composition is critical as it may affect the degradation behavior, as well as the mechanical properties since urea moieties are known to act as hard segments in poly(ester-urethane-urea) [24]. The FTIR and the μ-Raman analyses of the porous PCLU scaffold and the non-porous material exhibits characteristic bands of poly(ester-urethane)-based material (Fig. 1(c) and 1(d)) [12]. Indeed in the μ-Raman spectrum (Fig. 1(d)), it is possible to identify the following chemical groups for the non-porous material [25, 26]: stretching of urethane NH groups shifted by H-bonding at 3385 cm^{-1}, asymmetric and symmetric stretching of CH_2 groups at 2925, 2870 and 2740 cm^{-1}, stretching of urethane and ester free $C{=}O$ groups at 1731 cm^{-1} and hydrogen-bonded $C{=}O$ groups for the shoulder of the peak at 1639 cm^{-1}, bending of urethane NH group and stretching of CN groups at 1544 cm^{-1}, bending of CH_2 groups at 1451 and 1372 cm^{-1}, and stretching of CN and CO groups at 1304 cm^{-1}. For the porous PCLU scaffold, it was also identified two additional peaks attributed to urea $C{=}O$ and $NH{-}C{=}O$ groups at 1650 and 1620 cm^{-1}. μ-Raman spectroscopy is very interesting for further scaffold analysis since the technique allows the enhancement of polyurethane characterization and can be used to follow polyurethane degradation processes at a molecular level [25].

3.2. Determination of the scaffold quasi-static mechanical properties

Due to the presence of additional urea moieties in the structural composition of PCLU scaffolds, it is necessary to confirm the retention of the elastomeric behavior. Therefore, the quasi-static mechanical properties were determined through compression tests. In an uni-axial stress mode

Biomedical Optics EXPRESS

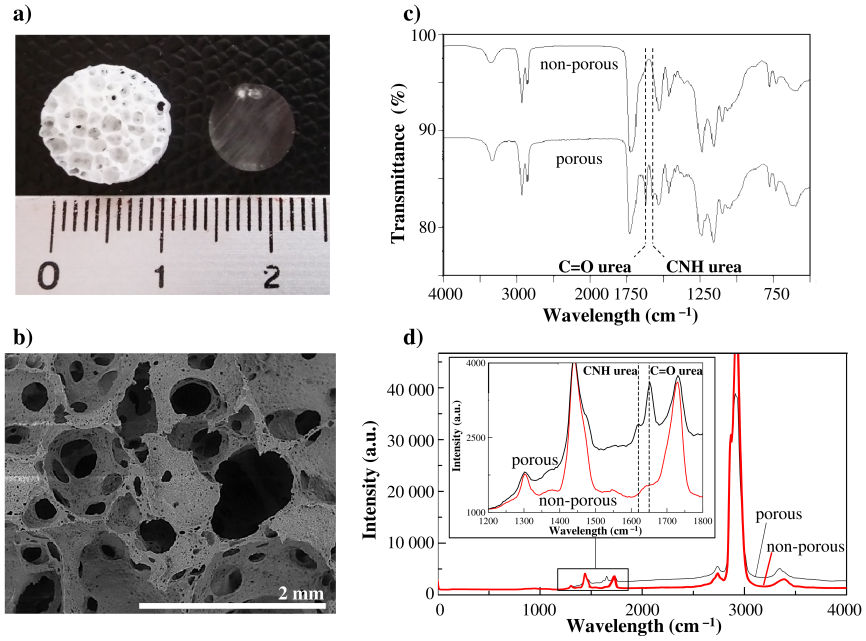

Fig. 1. (a) Photography of the porous PCLU scaffold (left) and non-porous material (right); (b) ESEM image of the porous PCLU scaffold; (c) FTIR-ATR analysis of the non-porous material and the porous PCLU scaffold; (d) μ-Raman analysis of the non-porous material and the porous PCLU scaffold. (dotted lines indicate urea functions).

of compression, that is to say when the scaffold only developed stresses in the compression direction and expanded freely in the two other directions, a typical compressive stress-strain response of an elastomeric open-cell foam was found (Fig. 2(a)) [27]. At the beginning of the stress-strain curve, the stress depends linearly on the strain and it is possible to determine the effective elasticity modulus E_1^* of the porous scaffold (Fig. 2(b)). Then, the post-buckling domain is characterized by a long elastic plateau due to pores collapse. Finally, strain increases dramatically when the densification is reached and it is possible to determine the elastic modulus of the related non-porous material ($E_{non-porous}$) (Fig. 2(a)).

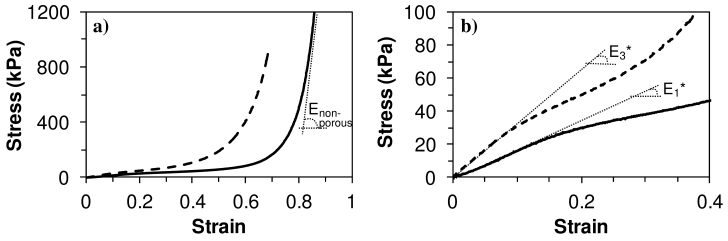

Fig. 2. Mechanical behavior of the PCLU scaffold under uni-axial (solid line) and tri-axial (dotted line) stress modes of compression: (a) all strain range; (b) low strain range.

The compression test gave values of 16 ± 2 MPa for $E_{non-porous}$ and 161 ± 14 kPa for E_1^* at a frequency 1/10 Hz corresponding to the acquisition time of the linear slope. For comparison,

Biomedical Optics EXPRESS

the nanoindentation tests of the non-porous material provided Young modulus of 49 ± 7 MPa, 42 ± 7 MPa and 35 ± 8 MPa, for 45 Hz, 10 Hz and 1 Hz frequencies, respectively, at a fixed strain rate of 0.05 s^{-1}. Typical load and unload force-displacement curves are shown in Fig. 3 and evidence the stiffening as the frequency is increasing.

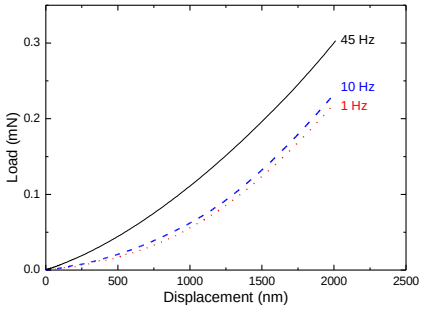

Fig. 3. Load-displacement curves of the dense PCLU from nanoindentation tests for three different frequency (1 Hz, 10 Hz and 45 Hz) and a fixed strain rate of 0.05 s^{-1}.

The effective elasticity modulus E_1^* found for the PLCU scaffold is in good agreement with the expected theoretical value E_{1theo}^* (E_{1theo}^* = 165 kPa with N = 2.4) evaluated using Eq. (10) [28]:

$$E_{1theo}^* = E_{non-porous} \times (1 - P)^N \tag{10}$$

where P is the porosity of the scaffold (P = 85.1%), and N is an exponent value which varies between 1 and 3 depending on pore shape and orientation.

Moreover, the number average molecular weight between cross-links $\bar{M_c}$ of the PCLU scaffold can be evaluated according to the theory of the rubber elasticity using using Eq. (11) [29]:

$$\bar{M_c} = \frac{3\rho RT}{E_1^*} \tag{11}$$

where ρ is the PCLU scaffold density (159 $kg.m^{-3}$), R is the universal gas constant, and T is the absolute temperature. The number average molecular weight between cross-links was found to be 7340 $g.mol^{-1}$ which is in good agreement with the value found by the swelling experiments ($\bar{M_c}$ = 7930 ± 1600 $g.mol^{-1}$).

The mechanical properties of the PLCU scaffold were also studied when confining the scaffold in a hole to mimic the containment to which the material can be subjected after implantation in cavitary defects. Therefore, the scaffold developed stresses in all directions. As expected for the tri-axial stress mode of compression, the stress-strain curve is similar to that under uni-axial stress mode of compression (Fig. 2(a)); but the compressing requires larger stresses. During tri-axial stress mode of compression, the effective elasticity modulus E_3^* was found to be 321 kPa (Fig. 2(b)), which is in good agreement with the theoretical modulus (E_{3theo}^* = 308 kPa with N = 2.4 and υ_* = 0.425) calculated using Eq.(12) [27]:

$$E_{3theo}^* = E_{non-porous} \times \frac{(1 - P)^N}{(2 - P) \times \left(1 - \frac{2\upsilon_*^2}{1-\upsilon_*}\right)} \tag{12}$$

where $E_{non-porous}$ is the elastic modulus of the non-porous material ($E_{non-porous}$ = 16 ± 2 MPa), P is the porosity of the scaffold (P = 85.1%), and υ_* is the Poisson′s ratio of the foam

Biomedical Optics EXPRESS

which varies between 0.1 and 0.4 for polymeric foams - it was found for instance to be 0.4 for polyester foams and 0.3-0.5 for polyurethane foams [30, 31]. We used a Poisson ratio $\nu = 0.425$ to convert the Young's modulus E measured at low frequency (compression and nanoindentation) to the longitudinal storage modulus $M' = E(1-\nu)/(1+\nu)/(1-2\nu)$, in order to compare later to the high frequency ones (ultrasonic and BLS). Finally, it is possible to conclude from the quasi-static mechanical tests that the porous PCLU scaffold behaves as elastomeric foam with appropriate elastic modulus for soft tissue regeneration [32].

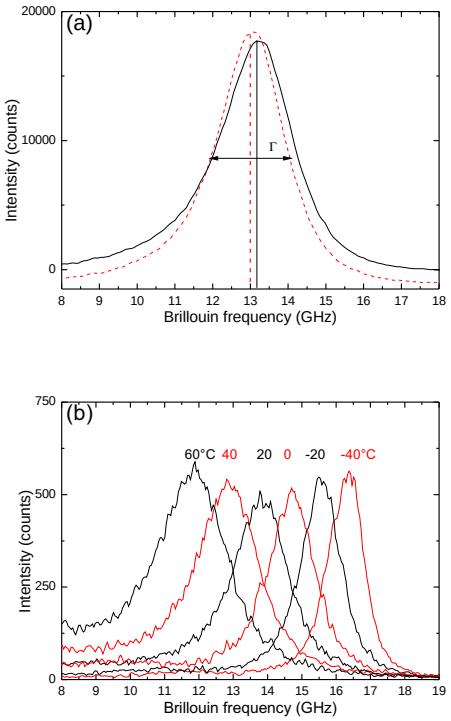

Fig. 4. (a) μ-Brillouin light scattering spectra of the non-porous material (dotted line) and the porous PCLU scaffold (solid line) at room temperature (20 °C). The peak is the inelastic scattering of the incident light by the longitudinal bulk acoustic wave with a Brillouin frequency shift $f_B \sim 13$ GHz. (b) μ-Brillouin light scattering spectra of the non-porous material as a function of the temperature (- 40 °C, + 60 °C).

3.3. *Determination of the scaffold dynamical viscoelastic properties by μ-Brillouin spectroscopy and ultrasound echoes*

A typical spectrum obtained at room temperature, is shown in Fig. 4(a) for the non-porous material and the porous PCLU scaffold. Their Brillouin frequency shift f_B lies close to 13 GHz while their full line-width at half-maximum are Γ_{porous}= 2140 MHz and $\Gamma_{non-porous}$ = 1873 MHz, respectively. We measured V_L = 2160 ± 110 m/s and the related longitudinal elastic modulus M' = 4.8 ± 0.4 GPa. The dynamical longitudinal viscosity η defined by Eq. (7), could be estimated from the natural line-width obtained after deconvolution of the instrument line-width, $\eta \sim$1.3 mPa.s. It is of the same order of magnitude as for soft glassy polymers [33] in the glassy state.

Biomedical Optics EXPRESS

These high-frequency results lead to a stiffer material than the ones measured by the ultrasonic pulse-echo method with a 10 MHz longitudinal transducer, V_L = 1773 ± 53 m/s and M' = 3.2 ± 0.15 GPa. We plotted the high frequency longitudinal storage modulus together with the quasi-static results in a log-log scale, as a function of the frequency, in Fig. 5. Finite relaxation time and low compressibility provide a qualitative explanation for the observed large difference in modulus between the ultrasound, Brillouin light scattering and quasi-static mechanical tests.

Indeed, recent rheological studies have shown that the mechanical modulus (M) of many soft materials follows a power-law dependence on frequency (f):

$$M = M_0(\frac{f}{f_0})^{\alpha} \tag{13}$$

Here, M_0 and f_0 are scale factors for stiffness and frequency, respectively, and α is the scaling exponent factor (α = 0 for purely elastic and 0 < α < 1 for viscoelastic materials) [34, 35]. $\alpha = x - 1$ can be related to the "noise temperature" x, introduced in the the soft glassy rheology (SGR) model [36]. Considering the Young modulus measured at low frequency (0.1 Hz–45 Hz), a best-fit provided α = 0.17 and $log(E_0/(f_0)^{\alpha}) = 2.48$. Our α value lies in the range 0.1 - 0.3 measured for several different cells in Ref. [34]. Additional information on the dynamical shear modulus G are needed to determine separately, the scale factors E_0 and f_0 [37].

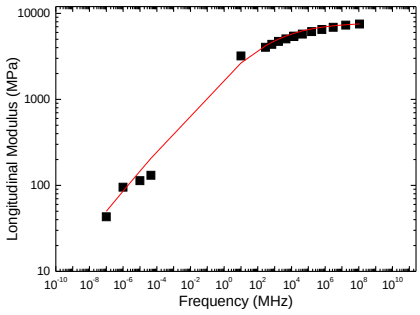

Fig. 5. Longitudinal storage modulus M' as a function of the frequency f (log-log scale) of the PCLU dense polymer. The line (red-color on-line) is a fit using the fractional derivative model described in the text.

For a more complete description of the modulus *vs* frequency behavior, a viscoelastic model is needed. The Cole-Davidson model [38], the Maxwell model [39] or the fractional derivative model [40] have been successfully employed to reproduce such behavior considering at least one relaxation time. In order to do such analysis, more data were necessary. We applied the time-temperature superposition principle to the temperature BLS results shown in Fig. 4(b) in combination with the employed viscoelastic model, described below. The horizontal translational parameter a_T defined by the two constants, C_1 = 11 K and C_2 = 225 K (see, Eq. (9)) was reasonably determined, ensuring an overall agreement between the viscoelastic model and the experiments (see Fig. 5).

In order to well interpret the storage modulus M' variation over the whole frequency range, using only a few number of parameters, we consider a fractional derivative model: the complex modulus reads

$$M^* = M_0 + M_1 \frac{(i\omega\tau)^{\alpha}}{1 + (i\omega\tau)^{\alpha}} \tag{14}$$

Biomedical Optics EXPRESS

With $M_0 \backsimeq 0$ (in fact, $M_0 << M_1$), $M_1 = 7.85$ GPa , $\alpha = 0.235$ and $\tau = 1$ ns, the calculated storage modulus variation $M' = \Re(M^*)$ *vs* frequency fits well the measurements (see Fig.5). According to this model, the modulus tends to the unrelaxed modulus $M_\infty = M_0 + M_1$ for frequencies much larger than τ^{-1}. This could explain the observed slow increase of M' for higher frequencies. Moreover for frequencies much smaller than τ^{-1}, the modulus variation can be fitted by a power law as previously discussed: for $M_0 \backsimeq 0$ and $\omega\tau << 1$, $M^* \approx M_1(i\omega\tau)^\alpha$

Supplementary information are still necessary, either on the loss-modulus M" and on the storage longitudinal modulus M' in the mHz–kHz range, in order to explore with more details the relaxation processes at lower frequency (< 0.1 Hz) and measuring the relaxed modulus M_0.

4. Conclusions

We demonstrated that PCLU scaffolds seem to possess the required mechanical features for soft tissue engineering since the quasi-static compression tests provided the effective Young modulus of the porous material, and confirmed the elastomeric behavior. The use of the ultrasonic at room temperature and μ-Brillouin inelastic light scattering as a function of the temperature (- 40 °C, + 60 °C) provided a reasonable insight on the the high-frequency dynamical viscoelastic parameters and the relaxation time. The fractional derivative viscoelastic model with one single relaxation process successfully reproduced the longitudinal modulus evolution as a function of the frequency (0.1 Hz–100 THz). Moreover, combining μ-Raman and μ-Brillouin spectroscopies allowed to assess locally and simultaneously the chemical composition and the viscoelastic properties of the scaffold that does not differ significantly from the dense polymer. Therefore, the coupling of the two techniques should allow to establish relationship between local molecular variations and changes in mechanical properties during scaffold degradation, extra-cellular matrix deposition and cell adhesion.

Funding

Institute of Experimental Sciences of Université Paris 13 (BIO-POLYM and BIO-POLYM CELL projects) and PEPS-Mécanobiologie from CNRS (BRIPLASM project).

Disclosures

The authors declare that there are no conflicts of interest related to this article.

References

1. I.K. Ko, S.J. Lee, A. Atala, and J.J. Yoo, "In situ tissue regeneration through host stem cell recruitment," Exp. & Mol. Medicine **45**, e57 (2013).
2. Y. Tamada, and Y. Ykada, "Effect of preabsorbed proteins on cell adhesion to polymer surfaces," J. Colloid Interface Sci. **155**, 334–339 (1993).
3. F.P.W. Melchels, A.M.C. Barradas, C.A. van Blitterswijk, J. de Boer, J. Feijen, and D.W. Grijpma, "Effects of the architecture of tissue engineering scaffolds on cell seeding and culturing," Acta Biomater. **6**, 4208–4217 (2010).
4. M. Mastrogiacomo, S. Scaglione, R. Martinetti, L. Dolcini, F. Beltrame, R. Cancedda, and R. Quarto, "Role of scaffold internal structure on in vivo bone formation in macroporous calcium phosphate bioceramics," Biomaterials **27**, 3230–3237 (2006).
5. R.G.M. Breuls, T.U. Jiya, and T.H. Smit, "Scaffold stiffness influences cell behavior: opportunities for skeletal tissue engineering," The Open Orthop. J. **2**, 103–109 (2008).
6. H.-I. Chang, and Y. Wang, "Cell responses to surface and architecture of tissue engineering scaffolds," in " Regenerative medicine and tissue engineering - cells and biomaterials," D. Eberli, ed. (InTech, 2011).
7. S.-Y. Tee, J. Fu, C.S. Chen, and P.A. Janmey, "Cell shape and substrate rigidity both regulate cell stiffness," Biophys. J. **100**, L25–L27 (2011).
8. K.J.I. Ember, M.A. Hoeve, S.L. McAughtrie, M.S. Bergholt, B.J. Dwyer, M.M. Stevens, K. Faulds, S.J. Forbes, and C.J. Campbell, "Raman spectroscopy and regenerative medicine: a review," npj Regen. Medicine **2**, 12 (2017).
9. G. Antonacci, and S. Braakman, "Biomechanics of subcellular structures by non-invasive Brillouin microscopy," Sci. Reports **6**, 37217 (2016).

Biomedical Optics EXPRESS

10. P. Djemia, "La diffusion Brillouin pour caractériser les propriétés élastiques ou magnétiques de multicouches," in "Instrumentation, Mesure, Métrologie - Les ondes en instrumentation VOL 9/1-2," O. Elmazria, ed. (Hermes - Lavoisier, 2009).
11. Q. Chen, S. Liang, and G.A. Thouas, "Elastomeric biomaterials for tissue engineering," Prog. Polym. Sci. **38**, 584–671 (2013).
12. S. Changotade, G. Radu-Bostan, A. Consalus, F. Poirier, J. Peltzer, J.-J. Lataillade, D. Lutomski, and G. Rohman, "Preliminary in vitro assessment of stem cell compatibility with cross-linked poly(ϵ-caprolactone urethane) scaffolds designed through high internal phase emulsions," Stem Cells Int. **2015**, 283796 (2015).
13. G. Pallares, M. El Mekki Azouzi, M.A. González, J.L. Aragones, J.L.F. Abascal, C. Valeriani and F. Caupin, "Anomalies in bulk supercooled water at negative pressure," Proc. Natl. Acad. Sci. USA **111**, 7936 (2014).
14. L. Brannon-Peppas, and N.A. Peppas, "The equilibirum swelling behavior of porous and non-porous hydrogels," in "Absorbent polymer technology," L. Brannon-Peppas, and R.S. Harland eds. (Elsevier Science Publishers, 1990).
15. M. Barikani, and C. Hepburn, "Determination of crosslink density by swelling in the castable polyurethane elastomer based on 1/4-cyclohexane diisocyanate and para-phenylene diisocyanate," Iran. J. Polym. Sci. & Technol. **1(1)**, 1–5 (1992).
16. G. Rohman, D. Grande, F. Lauprêtre, S. Boileau, and P. Guérin, "Design of porous polymeric materials from interpenetrating polymer networks (IPNs): poly(DL-lactide)/poly(methyl methacrylate)-based semi-IPN systems," Macromolecules **38**, 7274–7285 (2005).
17. W.C. Oliver, G.M. Pharr, "Measurement of hardness and elastic modulus by instrumented indentation: advances in understanding and refinements to methodology," J. Mater. Res. **19**, 3–20 (2005).
18. J.D. Ferry, "Viscoelastic Properties of Polymers," (John Wiley & Sons, New Jersey, USA, 1980).
19. J. Dealy, D. Plazek, "Time-Temperature Superposition- a User's Guide," Rheol. Bull. **78**, 16–31 (2009).
20. L .Rouleau, J. -F. Deü, A. Legay and F. Le Lay, "Application of Kramers-Kronig relations to time-temperature superposition for viscoelastic materials," Mech. Mater. **65**, 66–75 (2013).
21. R. M. Guedes, "A viscoelastic model for a biomedical ultra-high molecular weight polyethylene using the time-temperature superposition principle," Polym. testing **30**, 294–302 (2011).
22. W. M. Madigosky, G. F. Lee and J. M. Niemiec, "A method for modeling polymer viscoelastic data and the temperature shift function," J. Acoust. Soc. Am. **119**, 3760–3765 (2006).
23. L. Rouleau, R. Pirk, B. Pluymers and W. Desmet, "Characterization and Modeling of the Viscoelastic Behavior of a Self-Adhesive Rubber Using Dynamic Mechanical Analysis Tests," J. Aerosp. Technol. Manag. São José dos Campos **7(2)**, 200–208 (2015).
24. J. W. Rosthauser, K. W. Haider, C. Steinlein, and C.D. Eisenbach, "Mechanical and dynamic mechanical properties of polyurethane and polyurethane/polyurea elastomers based on 4,4′-diisocyanatodicyclohexyl methane," J. Appl. Polym. Sci. **64(5)**, 957–970 (1997).
25. H. Janik, B. Pałys, and Z. S. Petrovic, "Multiphase-separated polyurethanes studied by micro-Raman spectroscopy," Macromol. Rapid Commun. **24(3)**, 265–268 (2003).
26. M. Chollet, and M. Horgnies, "Analyses of the surfaces of concrete by Raman and FT-IR spectroscopies: comparative study of hardened samples after demoulding and after organic post-treatment," Surf. Interface Analysis **43**, 714–725 (2011).
27. G. Ben-Dor, G. Mazor, G. Cederbaum, and O. Igra, "Stress-strain relations for elastomeric foams in uni-, bi- and tri-axial compression modes," Arch. Appl. Mech. **66**, 409–418 (1996).
28. Q. Hou, D. W. Grijpma, and J. Feijen, "Porous polymeric structures for tissue engineering prepared by a coagulation, compression moulding and salt leaching technique," Biomaterials **24**, 1937–1947 (2003).
29. J. Yang, A.R. Webb, S.J. Pickerill, G. Hageman, and G.A. Ameer, "Synthesis and evaluation of poly(diol citrate) biodegradable elastomers," Biomaterials **27**, 1889–1898 (2006).
30. R. Lakes, "Foam structures with a negative Poisson′s ratio," Sciences **235**, 1038–1040 (1987).
31. R.D. Widdle Jr., A.K. Bajaj, and P. Davies, "Measurement of the Poisson′s ratio of flexible polyurethane foam and its influence on a uniaxial compression model," Int. J. Eng. Sci. **46**, 31–49 (2008).
32. J. A. Burdick, and R. L. Mauck, " Biomaterials for tissue engineering applications," (Springer-Verlag, 2011).
33. D. Fioretto and F. Scarponi, "Dynamics of a glassy polymer studied by Brillouin light scattering," Mater. Sci. Eng., A **521-522**, 243–246 (2009).
34. B. Fabry, G.N. Maksym, J.P. Butler, M. Glogauer, D. Navajas, J.J. Fredberg, "Scaling the microrheology of living cells," Phys. Rev. Lett. **87**, 148102 (2001).
35. P. Sollich, F. Lequeux, P. Hébraud, M.E. Cates, "Rheology of soft glassy materials," Phys. Rev. Lett. **78**, 2020–2023 (1997).
36. P. Sollich, "Rheological constitutive equation for a model of soft glassy materials," Phys. Rev. E. **58**, 738–759 (1998).
37. G. Scarcelli, P. Kim, S. H. Yun, "In vivo measurement of age-related stiffening in the crystalline lens by Brillouin optical microscopy," Biophys. J. **101**, 1539–1545 (2011).
38. D. W. Davidson, R. H. Cole, "Dielectric Relaxation in Glycerine," J. Chem. Phys. **18**, 1417 (1951).
39. F. Renaud, J. L. Dion, G. .Chevallier, I. Tawfiq and R. Lemaire, "A New Identification Method of Viscoelastic Behavior: Application to the Generalized Maxwell Model," Mech. Syst. Signal Process. **25(3)**, 991–1010 (2011).
40. T. Pritz, "Five-Parameter Fractional Derivative Model for Polymeric Damping Materials," J. Sound Vib. **265(5)**, 935–952 (2003).